

A LONG TERM NORTH ATLANTIC WAVE HINDCAST

V.R Swail¹, V.J. Cardone² and A.T. Cox²

¹Environment Canada
Downsview, Ontario

²Oceanweather, Inc.
Cos Cob, CT

1. INTRODUCTION

The variability of the ocean wave climate of the North Atlantic (NA) Ocean has been studied in recent years using measured data (Bacon and Carter, 1991), and a long-term wave hindcast (WASA Group, 1995). However, the measured data suffer from gaps within the past four decades, are available at only a few locations and in some parts of the data base include visual observations. The wave hindcast was produced using operational wind fields spliced together from various sources and, therefore, does not provide homogeneous forcing for the wave model used, thereby rendering the results of the hindcasts inconclusive. Evidence has also been presented (Kushnir *et al.*, 1997) of a worsening of the wave climate in the eastern NA within the past few decades associated with North Atlantic Oscillation (NAO).

The objective of this study is to utilize the National Centers for Environmental Prediction (NCEP) global reanalysis (NRA) products (Kalnay *et al.*, 1996) to drive a third-generation wave model adapted to the NA on a high-resolution grid to produce a high-quality, homogeneous, long term wind and wave data base for assessment of trend and variability in the wave climate of the NA. To remove potential biases in the historical wind fields, all wind observations from ships and buoys are re-assimilated into the analysis

taking account of the method of observation, anemometer height and stability. Wind fields for all significant storms are kinematically reanalyzed with the aid of an interactive Wind Workstation (Cox *et al.*, 1995). Furthermore, high-resolution surface wind fields for all tropical cyclones, as specified by a proven tropical cyclone boundary layer model, are assimilated into the wind fields to provide greater skill and resolution in the resulting wave hindcasts.

Sections 2 and 3 of this report describe the wave model used in the hindcast, and the wind fields used to drive the wave model; Section 4 describes how the long-term production hindcast was carried out. Section 5 shows preliminary results from comparative wind and wave climatologies based on the hindcast and selected *in-situ* measurements for both sides of the North Atlantic.

2. WAVE MODEL

2.1 Physics

The wave model used for this hindcast is a discrete spectral type called OWI 3-G. The spectrum is resolved at each grid point in 24 directional bins and 23 frequency bins. The bin centre frequencies range from 0.039 Hz to 0.32 Hz increasing in geometric progression with a constant ratio 1.10064. Deep-water physics is assumed in both the propagation

algorithm and the source terms. The propagation scheme (Greenwood *et al.*, 1985) is a downstream interpolatory scheme that is rigorously energy conserving with great circle propagation effects included. The source term formulation and integration is a third-generation type (WAMDI, 1988) but with different numerics and with the following modifications of the source terms in official WAMDI. First, a linear excitation source term is added to the input source term to allow the sea to grow from a flat calm condition without an artificial warm start sea state. The exponential wind input source is taken as the Snyder *et al.* (1981) linear function of friction velocity, as in WAMDI. However, unlike WAM, in which friction velocity is computed from the input 10-m wind speed following the drag law of Wu (1982), a different drag law is used in OWI 3-G. That law follows Wu closely up to wind speed of 20 m/s and then becomes asymptotic to a constant at hurricane wind speeds. The dissipation source term is taken from WAMDI except that the frequency dependence is cubic rather than quadratic. Finally, the discrete interaction approximation to the non-linear source term is used as in WAMDI except that two modes of interaction are included (in WAMDI the second mode is ignored). Further details on this model and its validation may be found in Khandekar *et al.* (1994) and Cardone *et al.* (1996).

2.2 Adaptation to North Atlantic

OWI 3-G is adapted on a latitude-longitude grid consisting of a 122 (in latitude) by 126 (in longitude) array of points. The grid spacing is 0.625° in latitude by 0.833° in longitude, which is within 10% of square (i.e. $\Delta x = \Delta y$) between 38° and 45° N. After deductions for land there are 9023 grid points, as shown in Figure 1. The south edge of the grid is at the equator. This boundary is treated as open. Time histories of two-dimensional spectra are prescribed at all grid points along the equator

as interpolated from the output of a lower resolution global first generation model driven by unmodified NCEP reanalysis 10 m wind fields. The eastern boundary is at 20° E longitude and the northern boundary is at 75.625° N latitude. The basic model integration time step is 0.5 hours and consists of one 30 propagation time step and two 15 minute growth cycles.

This wave model has been shown to reproduce observed wave heights very well when driven by accurate wind fields (Cardone *et al.*, 1995, 1996).

3. WIND FIELDS

In the production phase of the project, currently underway, the NCEP surface winds are brought into the Wind WorkStation every 6 hours in monthly segments for evaluation by a trained marine-meteorologist. The NCEP surface (10 m) wind fields on the Gaussian grid were identified in the evaluation phase of this project, described elsewhere in this volume by Cox *et al.* (1998), as being the most appropriate to drive the North Atlantic wave hindcast model. The NCEP surface winds are further refined by computing an equivalent neutral wind using the NCEP 2m surface temperature and sea-surface temperature fields and the algorithm described by Cardone *et al.* (1990). All available marine surface data, including buoy observations, ship reports (from COADS), C-MAN stations and ERS 1/2 scatterometer winds are displayed and selectively assimilated (as determined by the analyst) into the final wind field. All wind observations are subjected to a vigorous quality control and are adjusted for height and stability. Altimeter measurements are adjusted as recommended by Cotton and Carter (1994).

Winds for tropical systems are generated using a proven tropical cyclone model as

described by Cardone *et al.* (1994) and Thompson and Cardone (1996). Track and initial estimates of intensity are taken, with some modification, from the NOAA Tropical Prediction Center's (TPC) HURDAT database. The radius of maximum wind is determined using a pressure profile fit to available surface observations and aircraft reconnaissance. Reconnaissance data are taken from TPC's Annual Data and Verification Tabulation diskettes from 1989-1996, digitally scanned from manuscript records for the period 1974-1988, and manually scanned from reconnaissance microfilm for periods prior to 1974. Figure 3 shows a pressure model fit to reconnaissance data adjusted to surface via Jordan (1957). Surface winds generated from the model are then evaluated against available surface data and aircraft reconnaissance wind observations adjusted to the surface as described by Powell *et al.* (1989). Model winds within 240 nautical miles from the centre are then exported on a 0.5° latitude/longitude grid for inclusion in the Wind WorkStation.

The interactive hindcast methodology used by the analysts follows similar previous hindcast studies (Cardone *et al.*, 1995, 1996). Particular attention is spent on strong extratropical systems, blending tropical model winds into the NCEP surface wind field, and in the quality control of surface data. Kinematically analyzed winds from previous hindcasts of severe extratropical storms in the northwest Atlantic (Swail *et al.*, 1995) are incorporated into the present analysis on the North Atlantic wave model grid.

Altimeter measurements are used in an inverse wave-modelling approach as follows. First, a global coarse wave run is made and hindcast wave heights over the North Atlantic Ocean are compared to altimeter wave measurements. The global wave fields are generated using the Oceanweather wave

model adapted to a 1.25° by 2.5° latitude/longitude grid for the entire globe (Figure 4). NCEP surface winds (adjusted to neutral stability) are used to drive the global wave model. Areas where the resulting wave fields are deficient, as indicated by the altimeter, are brought to the analysts' attention and the analyst subjectively rectifies the deficiencies in the backward space-time evolution of the wind field causing the discrepancy.

Final wind fields for each month were interpolated onto the 0.625° by 0.833° latitude-longitude wave model grid using the IOKA (Interactive Objective Kinematic Analysis) algorithm (Cox *et al.*, 1995) and then time interpolated to a one-hour timestep.

4. PRODUCTION HINDCAST

The production hindcast was carried out in monthly segments using the OWI 3-G wave model in deep water mode driven by the final kinematically reanalysed wind fields as described above.

Final IOKA winds are run through the North Atlantic wave model as during the evaluation phase with the following modifications: First, a spectral save file is generated at the end of each month of integration and used to initialize the spectrum for the run of the succeeding month. Second, ice-cover is specified for each month from mid-monthly ice tables specified on the wave grid from Walsh & Johnson (1979) (prior to 1972), Arctic and Antarctic Sea Ice Data CD-ROM 1972-1994, and hand-digitized maps produced from the joint Navy/NOAA Ice Center data sets. The 5/10 ice concentration contour was used as the definition of the ice edge - points with ice concentrations greater than 5/10 were considered as land by the model, those with concentrations 5/10 or less were considered as open water. Third, wave spectra from the

coarse global wave model noted above are used as boundary conditions along the equator. Wave spectra are saved along the equator every 2.5 degrees at a 3-hour time step and interpolated to the North Atlantic wave grid's time step and spatial resolution.

Quality control of the production hindcast consists mainly of comparisons of the wave hindcast against measurements evaluated against 12 deep-water buoys (Figure 2) and ERS 1/2 altimeter wave measurements.

The output of the model consists of 17 so-called 'fields' quantities (Table 1) at all grid points and the full two-dimensional spectrum at the 233 grid points shown in Figure 1. These points were selected to allow even coverage of the basin, as well as to allow the possibility to drive finer mesh models especially for the US East Coast, the Scotian Shelf and Grand Banks of Newfoundland and the European West Coast. Spectra were also output at the locations of selected moored buoys and offshore platforms.

5. PRELIMINARY RESULTS - CLIMATOLOGY

The following paragraphs describe various intercomparisons of the preliminary wind and wave climatology produced from the hindcast and from *in-situ* measurements on both sides of the North Atlantic ocean. The locations where the comparisons were carried out are shown in Figure 2.

At the time of writing hindcasts covering nearly 6 years had been completed (1990-1995). While this time period is not sufficient to accurately describe the real wind and wave climate at the selected locations, it is adequate to undertake some aspects of a comparative climatology of hindcasts versus

measurements; however, it is not yet long enough to compare extremal analysis results, or to evaluate possible climate trends and variability. Such analyses will have to wait until the completion of the full hindcast.

The hindcasts produced a continuous smoothly varying time series of winds and waves at each point on the grid; data were archived at 6-hour intervals for the climatology.

The measured data came from a variety of sources. U.S. buoy data came from the NOAA Marine Environmental Buoy Database on CD-ROM; the Canadian buoy data came from the Marine Environmental Data Service marine CD-ROM; the remaining data came from the Comprehensive Ocean Atmosphere Data Set (COADS). The wave measurements are comprised of 20-minute samples (except for Canadian buoys which were 40 minutes) once per hour. The wind measurements were taken as 10 minute samples, scalar averaged, except vector averaged at the Canadian buoys, also once per hour. The wind and wave values selected for comparison with the hindcast were 3-hour mean values centered on each six hour synoptic time with equal (1,1,1) weighting. The wind speeds were adjusted to 10 m neutral winds in both the measured and hindcast data.

The measured data sets contained some gaps and some erroneous data. Where a gap existed in the measured data the corresponding data from the hindcast were ignored. There were many obvious spikes (high and low) in the measured data, particularly from the eastern Atlantic data sets accessed from COADS, or otherwise bad or suspicious data. These data points were removed along with the corresponding hindcast data. There may still remain more subtle errors in some measurements, in spite of our best efforts to identify and remove them. Removal of the

hindcast data corresponding to measurements gaps is necessary to achieve a valid intercomparison between hindcast and measurements; as a result, however, the climatologies may not be an accurate depiction of the “true” climatic conditions of the 6-year period 1990-95.

A series of comparative climate statistics for 8 of the locations shown in Figure 2 is given in Table 2, for significant wave height (HS), wind speed (WS) and spectral peak period (TP). A discussion of the climate comparisons is given in the following sections.

5.1 Wave Height Climatology Comparisons

From Table 2 it is clear that the hindcast represents the wave climate very well at the selected locations. The hindcast mean wave heights typically exceed the measurements by a few centimetres. The standard deviations are also very closely approximated, with the buoy measurements being slightly more variable than the hindcasts, and the platforms slightly lower. The higher order moments of the distribution are also remarkably close, except at 44011, where the distribution deviates in both skewness and kurtosis, likely a reflection of the relatively shallow water depths surrounding the buoy. In all cases the skewness and kurtosis of the hindcast waves exceeds that of the measurements. The 90, 95 and 99 percentile wave heights are typically within a few centimetres at the buoys, with the measurements tending usually to be slightly higher than the hindcasts; at the platforms the model is noticeably higher than the measurements. Comparisons of the maximum hindcast and measured waves shows no clear pattern. In some cases the measurements are higher, most notably at 44137 where the 15.8 m maximum came from the Halloween storm documented by Cardone *et al.* (1996), which showed an inability of all the models tested to reproduce the extreme wave heights generated

by the storm. Generally, except for 44011 and LF5U, the differences in the wave height maxima were less than 1 m.

Figure 5 shows quantile-quantile plots for model versus measured wave height for each of the 8 selected sites. In quantile scatterplots, the quantiles of one variable are plotted against the quantiles of another variable in order to assess the similarity of the empirical distributions of the two variables. If the data points fall on the regression line, then it can be concluded that the two variables follow the same distribution. Q-Q plots are particularly useful in comparisons of the right-hand (extreme) tails of the distributions. These plots show very good agreement across the entire frequency distribution. There is a slight tendency for the model to overestimate the wave height compared to the measurements for low values of sea state. The model also is consistently higher at the platforms, although the differences are negligible for the few highest observations. The effect of the Halloween storm is clearly seen at 44137 and 44138, where the peak measured waves clearly exceed the hindcast values. At 44011, in relatively shallow water, the 8 points for which the model greatly exceeds the measured wave heights all come from the same 48-hour period during the extreme Halloween storm.

5.2 Wind Speed Climatology Comparisons

The hindcast and measured wind speed climatologies are not independent since all of the wind data used contributed heavily to the data assimilation scheme in the NCEP re-analysis, and again in the kinematic re-analysis. Nevertheless, it is useful to compare the two data sets to verify that the various adjustments for elevation and interpolation onto the wave model grid have not compromised the hindcast data set.

Table 2 shows that the mean wind speeds are within a few cm/s, except at the two platforms where the differences are about 0.6-0.7 m/s; the model mean winds were generally equal to or slightly higher at all locations. The wind speed standard deviations were quite similar with the measured winds being slightly more variable. As for waves, the higher order moments were also comparable, with the hindcast having consistently higher values of skewness and also higher kurtosis except at the platforms. The 90, 95 and 99 percentile wind speeds were nearly identical, although the model winds at the platforms were 0.6-0.7 m/s higher than the measurements. There were some differences in the maximum wind speeds, split evenly between the two data sources as to which was higher. Differences were typically on the order of 2-3 m/s.

Figure 6 shows quantile-quantile plots for model versus measured wind speed for each of the 8 selected sites. These plots show very good agreement across the entire frequency distribution. There is a tendency for the model winds to be slightly higher at the Canadian buoys, particularly for the highest wind speeds, possibly related to the vector averaging of the buoy wind samples as opposed to scalar averages elsewhere. There is also a noticeable difference in the highest values at 44011, with the hindcast values exceeding the buoy. However, as for the wave height the top 8 values were all associated with the Halloween storm. At the platforms the model is noticeably higher than the measurements for the low end of the wind speed distribution.

5.3 Wave Period Climate Comparisons

The wave period comparisons were particularly difficult to carry out. The spectral peak wave period is the reciprocal of the peak frequency. For the measurements this is computed from the one frequency band

containing the most energy. In bi-modal seas this may fluctuate from one value to another. The hindcast peak frequency is computed by taking the spectral density in each frequency bin, and fitting a parabola to the highest density and one neighbor on each side. If highest density is in the 0.32157 Hz bin, the peak period reported is the peak period of a Pierson-Moskowitz spectrum having the same total variance as the hindcast spectrum. Thus we are not comparing exactly equal quantities. Other problems relate to the measured data in the various archives. For the platforms and the 62108 buoy (the COADS-based observations) the wave period information was discretized into a very few bins (only 4 in one case). This made meaningful analysis very difficult. In the case of 41001 there were some problems with the measured data base which were not fully resolved. Therefore detailed analysis was only carried out at 4 sites (41010, 44011, 44137 and 44138).

Table 2 shows the statistics for all of the buoys. As noted above the information for the other 4 buoys should not be considered reliable. Some clear indications can be seen from the table. The means of the peak wave periods are consistently higher for the measurements than for the hindcast, by 0.5-1.5 seconds. The standard deviations of the measurements were also consistently higher. The skewness and kurtosis were usually higher for the measurements (except at 44011 in both cases). The 90, 95 and 99 percentile wave periods continued the low bias apparent in the hindcast mean period values with differences reaching almost 3 seconds in the 99 percentile value at the two Canadian buoys. Maximum values were similarly biased, although inexplicably the difference in the maxima for all except 41010 was less than the difference in the percentile values.

Figure 7 shows quantile-quantile plots for model versus measured spectral peak wave

period for each of the 4 sites considered to be relatively reliable. The shapes of the plots for the Canadian buoys (44137, 44138) show a small but consistent bias even in the lowest periods, growing slowly to periods of about 11s, then growing more quickly. However, for the few highest values of peak period the measurement is only slightly larger than the model values. Buoy 44011 shows a similar tendency, although without the relatively large bias at longer periods demonstrated by the other two. For buoy 41010 the bias grows more quickly from the outset, and continues to grow rapidly; unlike the other 3 buoys the maxima are widely divergent. A more detailed analysis of the reasons for this behaviour is required.

6. SUMMARY AND FUTURE WORK

In summary, a comprehensive wind and wave hindcast is presently being produced for the North Atlantic Ocean using a long term, consistent wind field forcing based on the NCEP re-analysis. The NCEP surface wind fields are kinematically re-analysed to reproduce small-scale features such as tropical storms and to reduce the inherent low bias in extreme extratropical storms due to the limited grid resolution in the NCEP wind fields. The wind fields are used to drive a 3rd generation wave model on a fine mesh grid covering the entire North Atlantic Ocean. The output from the wave model, consisting of 17 different fields is archived at 6-hour intervals at each grid location; 2-D wave spectra are archived every 6 hours at 233 grid points covering the entire basin, but particularly along the continental margins.

The wind speed and wave height climatology produced from the hindcast closely resembles that obtained from measured wind and wave data from buoys and offshore platforms on both sides of the Atlantic Ocean, in terms of the various statistical moments and the shape

and scale of the frequency distributions. This confirms that the wave hindcast results may be used as a high-quality estimate of the actual wave climate.

The full wave hindcast should be completed in late 1998, thus providing a high-quality, long-term homogeneous data base of winds and waves over the entire North Atlantic Ocean. At that time more extensive climate analysis, including an investigation of the trend and variability of North Atlantic wave heights, and an extremal analysis of waves can be carried out. Investigation of the spatial patterns of wave height variability and relationships to large scale circulation features such as the North Atlantic Oscillation is also planned.

7. REFERENCES

- Bacon, S., and D.J. Carter, 1991. *Wave climate changes in the North Atlantic and North Sea*. Int. J. Climatology, 11, 545-558.
- Cardone, V.J., J.G. Greenwood and M.A. Cane, 1990. *On trends in historical marine wind data*. J. Climate, 3, 113-127.
- Cardone, V.J., A.T. Cox, J.A. Greenwood, and E.F. Thompson, 1994. *Upgrade of tropical cyclone Surface wind field model*. U.S. Corps of Engineers Misc. Paper CERC-94-14.
- Cardone, V.J., H.C. Graber, R.E. Jensen, S. Hasselmann, and M.J. Caruso, 1995. *In search of the true surface wind field in SWADE IOP-1: ocean wave modelling perspective*. The Global Ocean Atmosphere System, 3, 107-150.
- Cardone, V.J., R.E. Jensen, D.T. Resio, V.R. Swail and A.T. Cox, 1996. *Evaluation of contemporary ocean wave models in rare extreme events: "Halloween storm of October, 1991; "storm of the century" of March, 1993"*.

- J. Atmos. and Oceanic Tech., Vol. 13, No. 1, p. 198-230.
- Cotton, P.D., and D.J.T. Carter, 1994. *Cross calibration of TOPEX, ERS-1, and Geosat wave heights*. J. of Geophysical Research, Vol 99, No. C12, pp. 25,025-25,033.
- Cox, A.T., J.A. Greenwood, V.J. Cardone and V.R. Swail, 1995. *An interactive objective kinematic analysis system*. Proceedings 4th International Workshop on Wave Hindcasting and Forecasting, October 16-20, 1995, Banff, Alberta, p. 109-118.
- Cox, A.T., V.J. Cardone and V.R. Swail, 1998. *Evaluation of NCEP/NCAR reanalysis project marine surface wind products for a long term North Atlantic wave hindcast*. Proc. 5th International Workshop on Wave Hindcasting and Forecasting, Melbourne, FL
- Greenwood, J.A., V.J. Cardone and L.M. Lawson, 1985. *Intercomparison test version of the SAIL wave model*. Ocean Wave Modelling, the SWAMP Group, Plenum Press, 221-233.
- Jordan, C.L. 1957. *Estimation of surface central pressures in tropical cyclones from aircraft observations*. Bull. AMS, Vol. 39, No. 7 pp.345-352.
- Kalnay, E., et al, 1996. *The NCEP/NCAR 40-Year reanalysis project*. Bull. AMS, 77(3), 437-471.
- Khandekar, M.L., R. Lalbeharry and V.J. Cardone, 1994: *The performance of the Canadian spectral ocean wave model (CSOWM) during the Grand Banks ERS-1 SAR wave spectra validation experiment*. Atmosphere-Ocean 32(1), 31-60.
- Kushnir, Y. V.J. Cardone, J.G. Greenwood and M.A. Cane, 1997. *On the recent increase in North Atlantic wave heights*. Accepted in J. Climate.
- Kushnir, Y., 1994. *Interdecadal variations in North Atlantic sea surface temperature and associated atmospheric conditions*. J. Climate, 7, 141-157.
- Powell, M.D., and P.G. Black, 1989. *The relationship of hurricane reconnaissance flight-level wind measured by NOAA's oceanic platforms*. 6th National Conference on Wind Engineering, March 7-10, 1989.
- Snyder, R., F.W. Dobson, J.A. Elliott and R.B. Long, 1981. *Array measurements of atmospheric pressure fluctuations above surface gravity waves*. J. Fluid Mech., 102, 1-59.
- Swail, V.R., M. Parsons, B.T. Callahan and V.J. Cardone, 1995. *A revised extreme wave climatology for the east coast of Canada*. Proc. 4th International Workshop on Wave Hindcasting and Forecasting, October 16-20, 1995, Banff, Alberta, p. 81-91.
- Thompson, E.F., and V.J. Cardone, 1996. *Practical modeling of hurricane surface wind fields*. Journal of Waterway, Port, Coastal, and Ocean Engineering, July/August 1996, pp. 195-205.
- Walsh, J.E., and C.M. Johnson, 1979. *An analysis of Arctic sea ice fluctuations, 1953-1977*. J. Phys. Ocean., 9, 580-591.
- WAMDI Group, 1988. *The WAM model - a third generation ocean wave prediction model*. J. Phys. Ocean. 18: 1775-1810.
- WASA, 1995. *The WASA Project: changing storm and wave climate in the Northeast Atlantic and adjacent seas?* Proc. 4th International Workshop on Wave Hindcasting and Forecasting, Banff, Canada, October 16-20, 1995, 31-44; also: GKSS Report 96/E/61

Wu, J., 1982. *Wind-stress coefficients over the sea surface from breeze to hurricane*. J. Geophys. Res., (87), 9704-9706.

WS	Wind Speed	1-hour average of the effective neutral wind at a height of 10 metres, units in metres/second.
WD	Wind Direction	From which the wind is blowing, clockwise from true north in degrees (meteorological convention). Winds are 1-hour averages of the effective neutral wind at a height of 10 metres.
ETOT	Total Variance of Total Spectrum:	The sum of the variance components of the hindcast spectrum, over the 552 bins of the 3G wave model, in metres squared.
TP	Peak Spectral Period of Total Spectrum:	Peak period is the reciprocal of peak frequency, in seconds. Peak frequency is computed by taking the spectral density in each frequency bin, and fitting a parabola to the highest density and one neighbor on each side. If highest density is in the .32157 Hz bin, the peak period reported is the peak period of a Pierson-Moskowitz spectrum having the same total variance as the hindcast spectrum.
VMD	Vector Mean Direction of Total Spectrum	To which waves are traveling, clockwise from north in degrees (oceanographic convention).
ETOT1	Total Variance of Primary Partition	The sum of the variance components of the hindcast spectrum, over the 552 bins of the 3G model, in metres squared. To partition sea (primary) and swell (secondary) we compute a P-M (Pierson-Moskowitz) spectrum, with a \cos^3 spreading, from the adopted wind speed and direction. For each of the 552 bins, the lesser of the hindcast variance component and P-M variance component is thrown into the sea partition; the excess, if any, of hindcast over P-M is thrown into the swell partition.
TP1	Peak Spectral Period of Primary Partition	
VMD1	Vector Mean Direction of Primary Partition	
ETOT2	Total Variance of Secondary Partition	
TP2	Peak Spectral Period of Secondary Partition	
VMD2	Vector Mean Direction of Secondary Partition	
MO1	First Spectral Moment of Total Spectrum	Following Haring and Heideman (OTC 3280, 1978) the first and second moments contain powers of $\omega = 2\pi f$; thus: $M1 = \sum \sum 2\pi f dS$ $M2 = \sum \sum (2\pi f)^2 dS$ where dS is a variance component and the double sum extends over 552 bins.
MO2	Second Spectral Moment of Total Spectrum	
HS	Significant Wave Height	4.000 times the square root of the total variance, in metres

Table 1. List of archived fields and definitions.

DMDIR	Dominant Direction	<p>Following Haring and Heideman, the dominant direction ψ is the solution of the equations</p> $A \cos 2 \psi = \sum \sum \cos 2 \theta \pi \, dS$ $A \sin 2 \psi = \sum \sum \sin 2 \theta \pi \, dS$ <p>The angle ψ is determined only to within 180 degrees. Haring and Heideman choose from the pair $(\psi, \psi+180)$ the value closer to the peak direction.</p>
ANGSPR	Angular Spreading Function	<p>The angular spreading function is the mean value, over the 552 bins, of $\cos(\theta - \text{VMD})$, weighted by the variance component in each bin. If the angular spectrum is uniformly distributed over 360 degrees, this statistic is zero if uniformly distributed over 180 degrees, $2/\pi$ if all variance is concentrated at the VMD, 1.</p>
INLINE	In-Line Variance Ratio	<p>Called directional spreading by Haring and Heideman, p 1542. Computed as:</p> $\text{Rat} = \frac{[\sum \sum \cos^2(\theta - \psi) \, dS]}{[\sum \sum dS]}$ <p>If spectral variance is uniformly distributed over the entire compass, or over a semicircle, $\text{Rat} = 0.5$; if variance is confined to one angular band, or to two band 180 degrees apart, $\text{Rat} = 1.00$. According to Haring and Heideman, \cos^2 spreading corresponds to $\text{Rat} = 0.75$.</p>

Table 1 (cont.). List of archived fields and definitions.

	HS-model	HS-meas	WS-model	WS-meas	TP-model	TP-meas
	(m)	(m)	(m/s)	(m/s)	(sec)	(sec)
41001						
MEAN	1.96	1.96	7.69	7.55	5.29	6.47
STDEV	1.02	1.08	3.52	3.56	0.77	1.66
COEF_VAR	0.52	0.55	0.46	0.47	0.15	0.26
SKEW	1.89	1.72	0.64	0.51	1.35	1.38
KURT	5.31	4.19	0.25	0.06	3.09	2.62
MAX	9.27	10.00	23.60	23.89	10.05	16.50
90%ILE	3.28	3.47	12.51	12.39	6.27	8.50
95%ILE	3.99	4.10	14.32	14.03	6.75	10.50
99%ILE	5.45	5.63	17.12	16.92	7.87	12.50
41010						
MEAN	1.66	1.56	6.48	6.51	5.24	5.83
STDEV	0.79	0.83	3.08	3.13	0.74	1.08
COEF_VAR	0.47	0.53	0.47	0.48	0.14	0.18
SKEW	1.72	1.64	0.64	0.59	1.41	1.46
KURT	4.25	3.76	0.39	0.27	3.87	4.70
MAX	8.36	7.53	23.10	23.03	10.74	14.60
90%ILE	2.72	2.67	10.66	10.75	6.19	7.17
95%ILE	3.21	3.23	12.16	12.26	6.58	7.77
99%ILE	4.36	4.43	14.80	14.84	7.67	9.28
44011						
MEAN	1.95	1.96	6.58	6.38	5.46	5.81
STDEV	1.14	1.16	3.79	3.71	0.88	1.03
COEF_VAR	0.59	0.59	0.58	0.58	0.16	0.18
SKEW	2.27	1.70	0.80	0.71	1.21	0.88
KURT	10.08	4.21	0.51	0.27	2.47	1.14
MAX	13.99	11.43	27.59	25.28	10.85	10.97
90%ILE	3.48	3.53	11.93	11.61	6.61	7.17
95%ILE	4.22	4.30	13.74	13.33	7.10	7.73
99%ILE	5.92	5.89	16.84	16.44	8.20	8.87
44137						
MEAN	2.65	2.58	9.11	8.99	8.31	9.30
STDEV	1.50	1.55	4.35	4.45	1.84	2.16
COEF_VAR	0.57	0.60	0.48	0.50	0.22	0.23
SKEW	1.95	1.86	0.53	0.45	0.59	0.90
KURT	6.13	5.65	0.08	-0.13	0.37	0.99
MAX	15.09	15.80	28.73	28.38	17.59	17.87
90%ILE	4.51	4.57	15.08	15.09	10.78	12.20
95%ILE	5.49	5.63	16.87	16.98	11.72	13.56
99%ILE	8.12	7.90	20.38	20.27	13.03	15.93

Table 2. Comparison statistics for hindcast and *in-situ* climatology at selected sites.

	HS-model	HS-meas	WS-model	WS-meas	TP-model	TP-meas
	(m)	(m)	(m/s)	(m/s)	(sec)	(sec)
44138						
MEAN	2.69	2.67	8.67	8.57	8.86	10.22
STDEV	1.47	1.54	4.18	4.18	2.03	2.38
COEF_VAR	0.55	0.58	0.48	0.49	0.23	0.23
SKEW	2.05	1.77	0.70	0.57	0.53	0.69
KURT	6.79	5.03	0.55	0.21	0.29	0.68
MAX	13.43	13.40	29.27	26.35	17.62	21.33
90%ILE	4.52	4.65	14.40	14.21	11.62	13.50
95%ILE	5.46	5.66	16.27	16.21	12.54	14.78
99%ILE	8.36	8.00	20.16	19.84	14.13	17.09
62108						
MEAN	3.44	3.32	9.94	9.94	6.48	7.54
STDEV	1.82	1.87	4.53	4.62	1.18	1.70
COEF_VAR	0.53	0.56	0.46	0.46	0.18	0.23
SKEW	1.45	1.36	0.49	0.48	0.62	0.81
KURT	2.85	2.51	0.18	0.21	-0.04	0.56
MAX	13.55	13.50	33.78	34.45	10.65	14.50
90%ILE	5.83	6.00	15.89	15.92	8.16	10.50
95%ILE	6.86	7.00	17.77	17.84	8.68	10.50
99%ILE	9.64	9.70	22.03	22.11	9.64	12.50
LF3J						
MEAN	3.19	2.87	9.71	8.96	6.19	7.18
STDEV	1.84	1.70	4.67	4.77	1.14	1.28
COEF_VAR	0.57	0.59	0.48	0.53	0.18	0.18
SKEW	1.21	1.04	0.69	0.68	0.36	0.94
KURT	1.64	1.16	0.19	0.26	-0.60	3.13
MAX	11.89	12.00	32.08	30.05	10.05	18.50
90%ILE	5.70	5.00	16.16	15.52	7.77	8.50
95%ILE	6.72	6.00	18.49	17.80	8.20	8.50
99%ILE	9.11	8.00	22.23	21.80	8.85	10.50
LF5U						
MEAN	2.47	2.19	9.34	8.58	5.42	5.77
STDEV	1.54	1.33	4.17	4.24	1.03	1.00
COEF_VAR	0.62	0.61	0.45	0.49	0.19	0.17
SKEW	1.55	1.33	0.65	0.65	0.68	1.29
KURT	3.34	2.67	0.13	0.30	0.11	1.80
MAX	12.42	11.00	29.68	33.44	9.91	10.50
90%ILE	4.48	4.00	15.27	14.53	6.84	6.50
95%ILE	5.43	4.50	17.13	16.37	7.36	8.50
99%ILE	8.03	6.50	20.48	19.78	8.26	8.50

Table 2 (cont.). Comparison statistics for hindcast and *in-situ* climatology at selected sites.

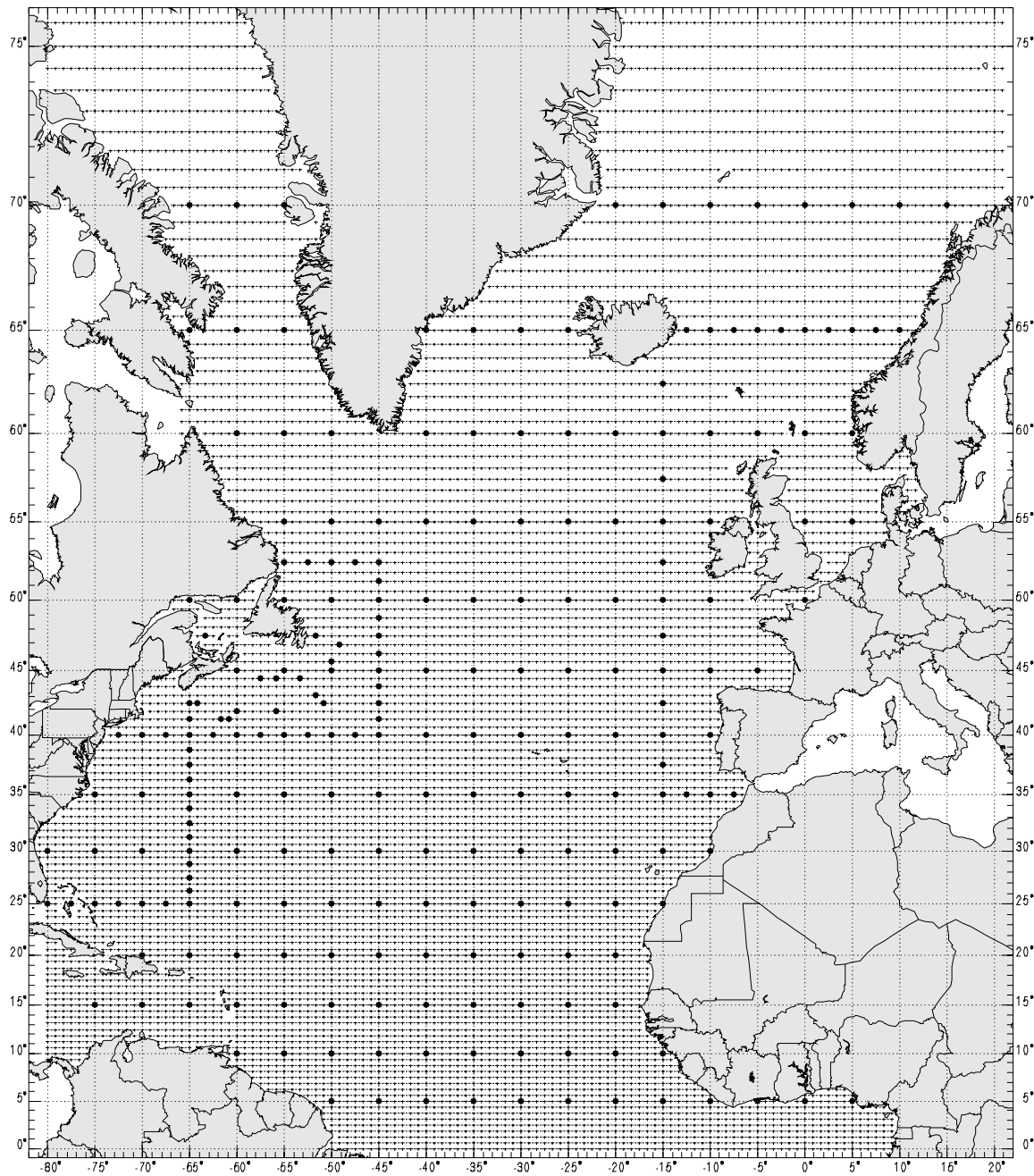


Figure 1. Wave Model Grid and Spectral Save Points

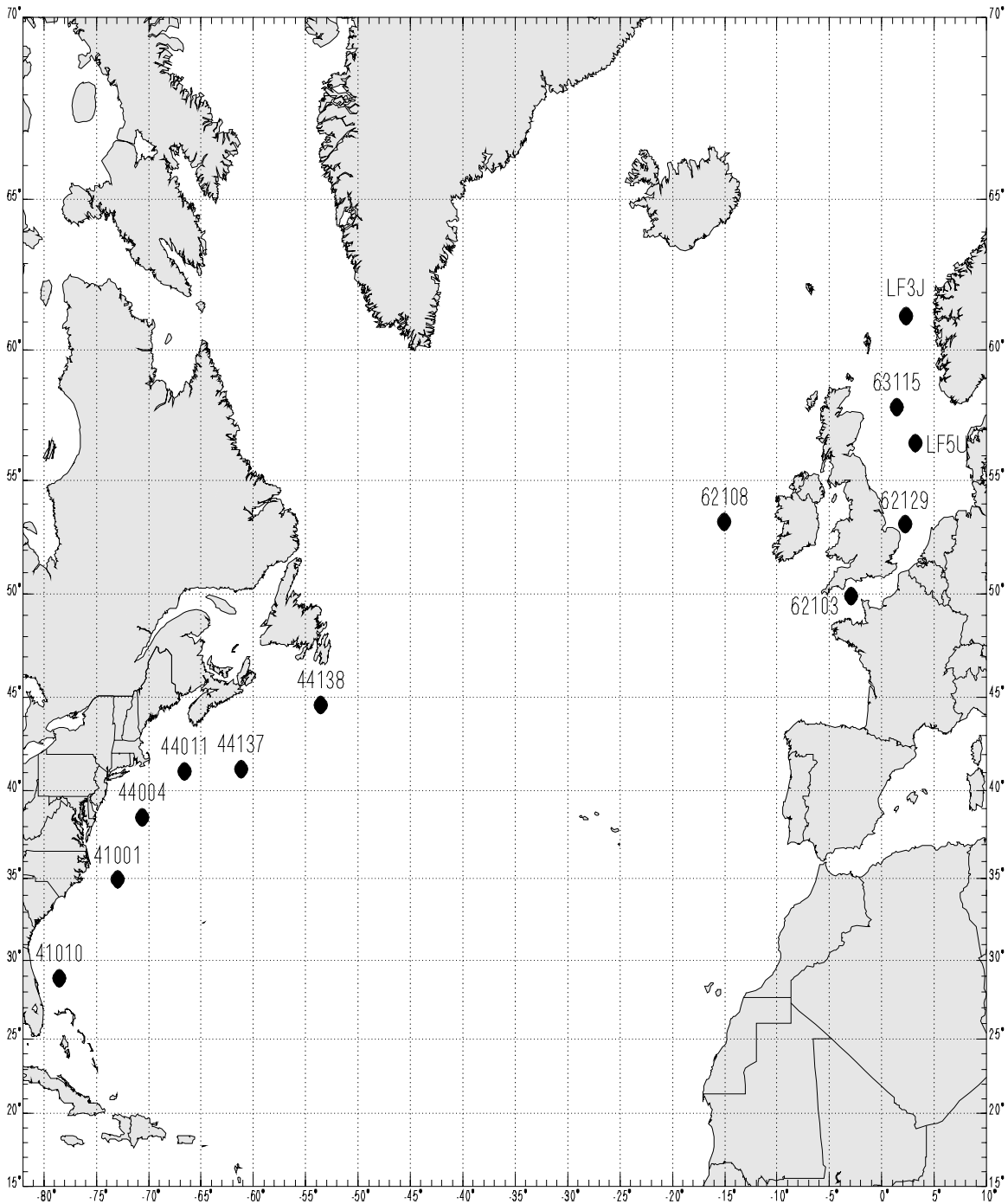


Figure 2. Locations of Wave Climatology Comparison Sites

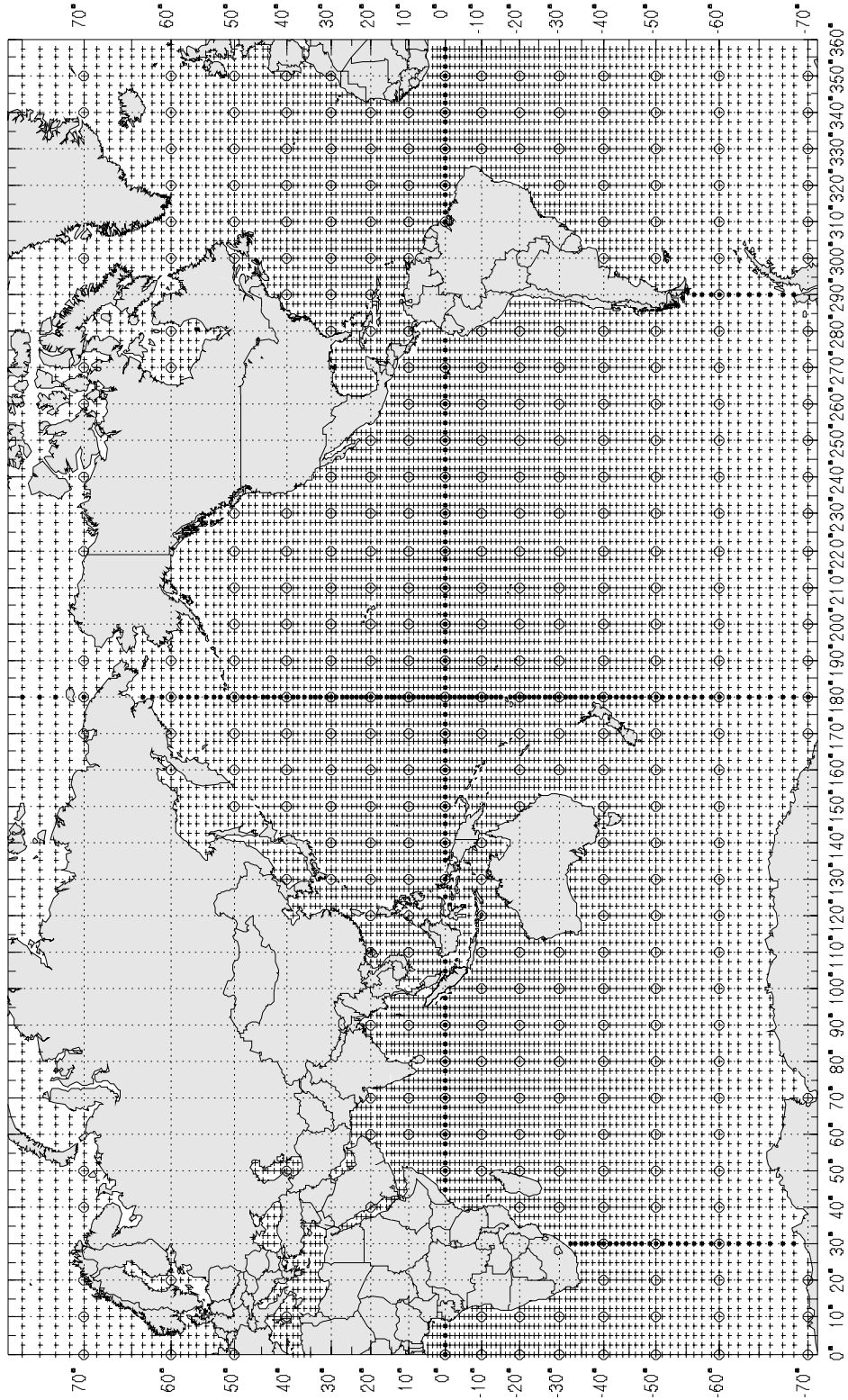


Figure 4. Global wave grid with spectral save points (circles).

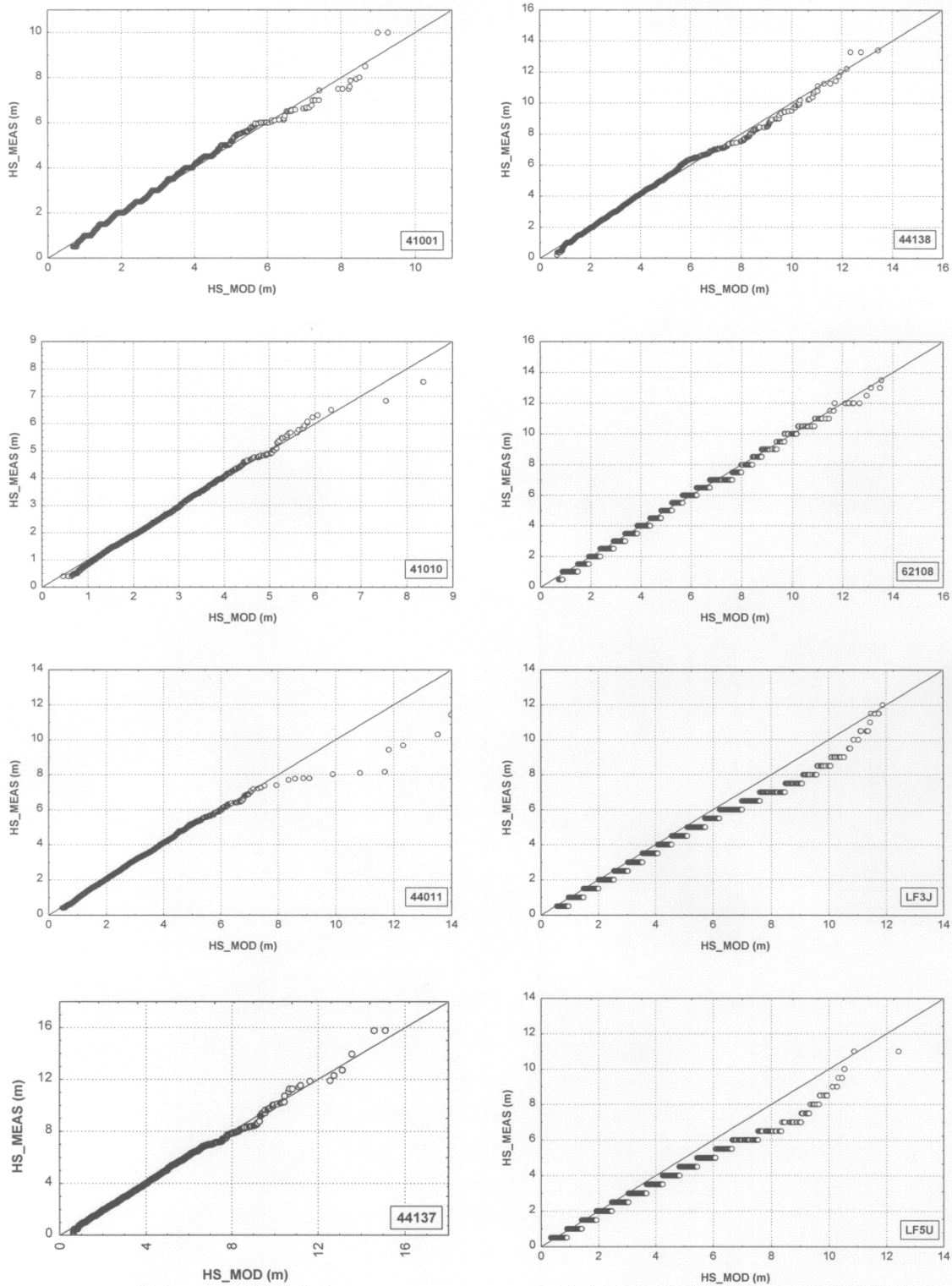


Figure 5. Q-Q plots of significant wave height for selected locations.

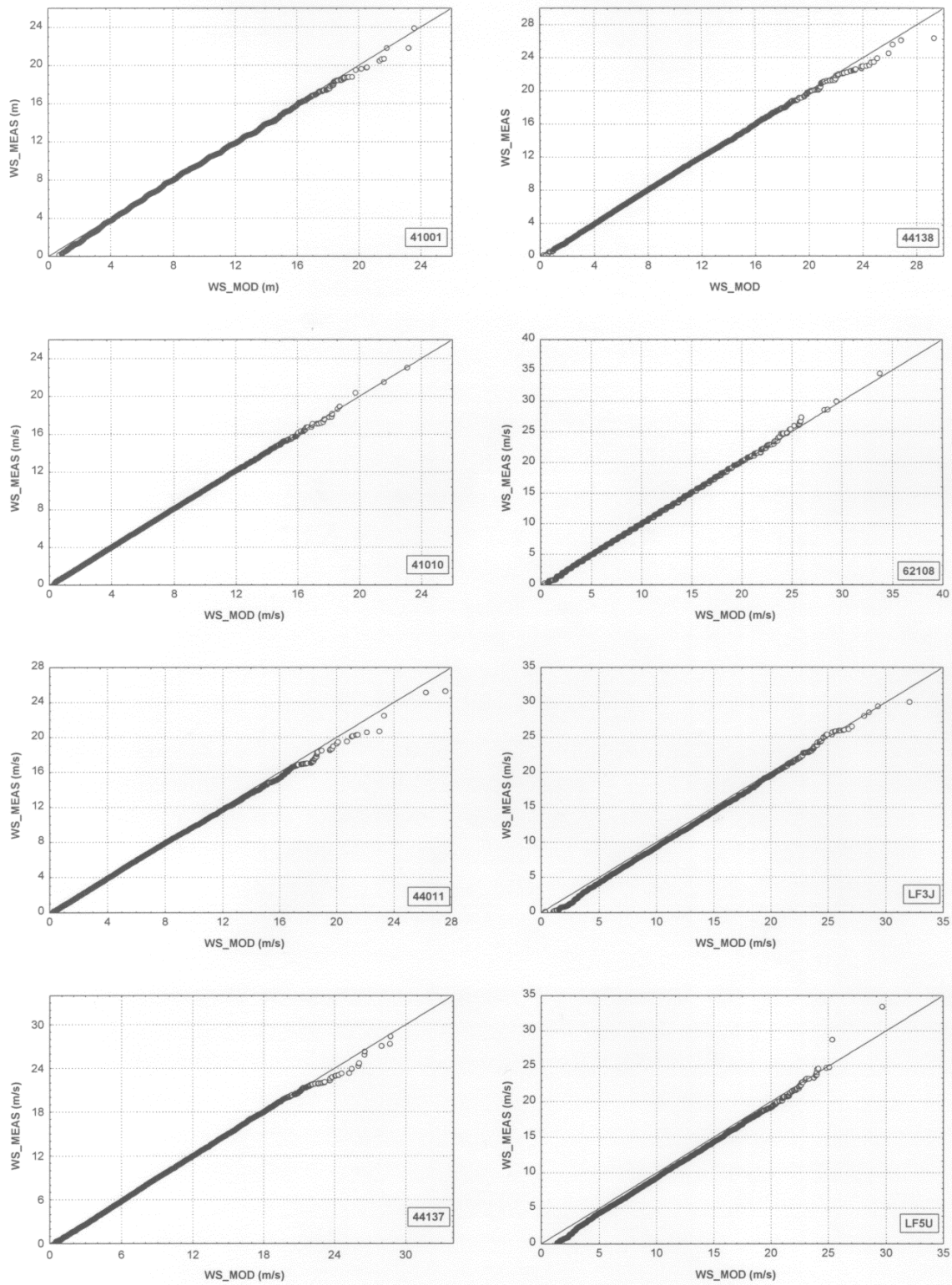


Figure 6. Q-Q plots of wind speed for selected locations.

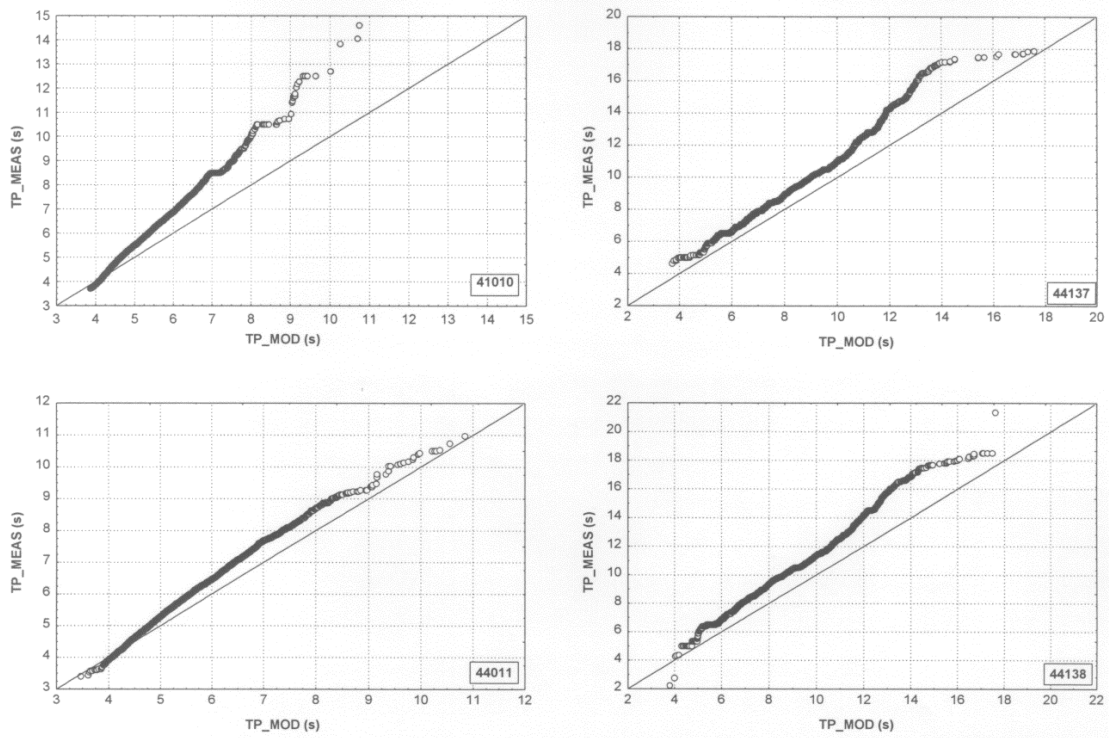


Figure 7. Q-Q plots of spectral peak wave period for selected locations.